The completed data table for well 4835-B is given in Table 2.2A and the plan view of the well is in Fig. 2.26A.

Table 2.2A. Data and calculated results from well 4835-B, Appleton field, Alabama. Kelly Bushing: 244 ft

Measured depth = log depth (ft)		True vertical depth (ft)	Depth subsea (ft)	Total rectangular coordinates (ft)	
0		0	244	0.00 N	0.00 E
928		928	–684	1.72 N	1.93 E
2308		2308	–2064	4.53 N	9.51 W
3282		3282	–3038	6.37 N	6.29 W
4150	Eutaw	4150	–3906	10.35 N	6.12 W
4400	U. Tuscaloosa	4400	–4156	11.50 N	6.07 W
4811		4811	–4567	13.38 N	5.99 W
4890	M. Tuscaloosa	4890	–4646	14.37 N	6.63 W
5150	L. Tuscaloosa	5150	–4906	17.64 N	8.75 W
5525	L. Cretaceous	5525	–5281	22.35 N	11.81 W
6198		6198	–5954	30.82 N	17.30 W
7696		7695	–7451	61.48 N	7.50 W
8328		8327	–8083	74.90 N	1.25 E
8482		8480	–8236	74.59 N	18.82 E
8661		8655	–8411	71.22 N	53.19 E
8935		8922	–8678	66.16 N	117.74 E
9186		9161	–8917	62.25 N	194.12 E
9556		9512	–9268	54.50 N	310.78 E
10006		9940	–9696	34.61 N	447.09 E
10266	Cotton Valley	10189	–9944	18.10 N	521.24 E
10431		10346	–10102	7.63 N	568.29 E
11103		10982	–10738	55.68 S	777.65 E
11621		11470	–11226	116.46 S	938.37 E
11960		11791	–11547	142.28 S	1045.58 E
12370	Haynesville	12178	–11934	168.39 S	1179.92 E
12450		12253	–12009	173.48 S	1206.13 E
12641		12432	–12188	185.03 S	1271.62 E
13020	Buckner	12789	–12545		
13072	Smackover[a]	12838	–12594	210.16 S	1414.16 E
13086		12851	–12607	210.98 S	1418.79 E
13190	OWC[b]		–12704	217 S	1453 E
13286	Base Smack		–12795	223 S	1485 E

[a] Attitude from dipmeter 12,056. [b] Oil-water contact.

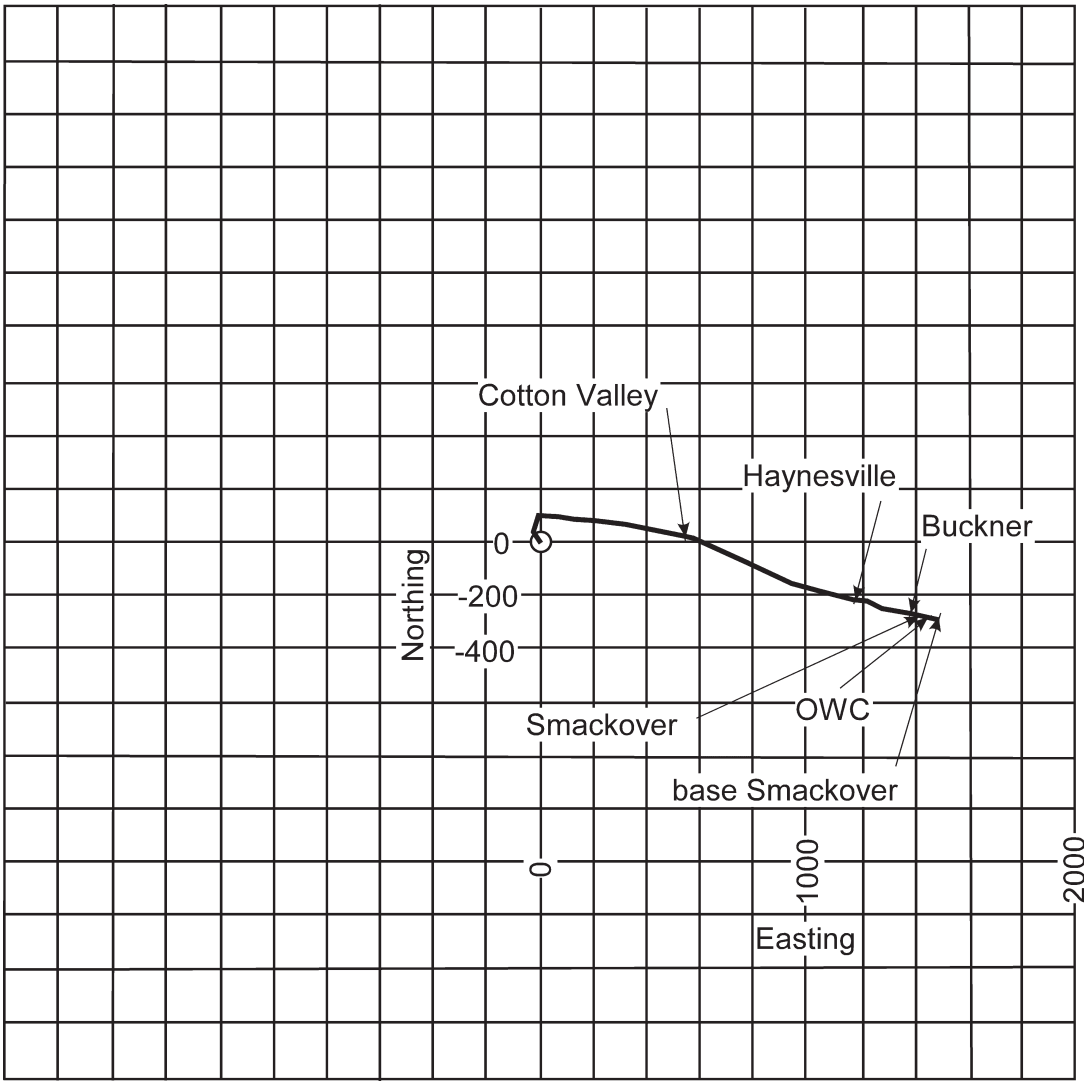

Fig. 2.26A. Plan view of Smackover well 4835-B (after Hawkins 1999)

The data in this exercise (Fig. 3.26) are the same as in Fig. 3.5. Possible interpretations are given in Figs. 3.9, 3.10a, 3.11b, 3.11c, 3.11d, 3.13b, 10.3b. Numerical data for this exercise are in text file "03-05dat.txt."

The data in this exercise (Fig. 3.27) are mapped and discussed in Fig. 10.10.

The interpretation is given in Fig. 3.29A. Because this is a relatively smooth surface, it indicates that the locations of the different contacts from which it was constructed must be about correct.

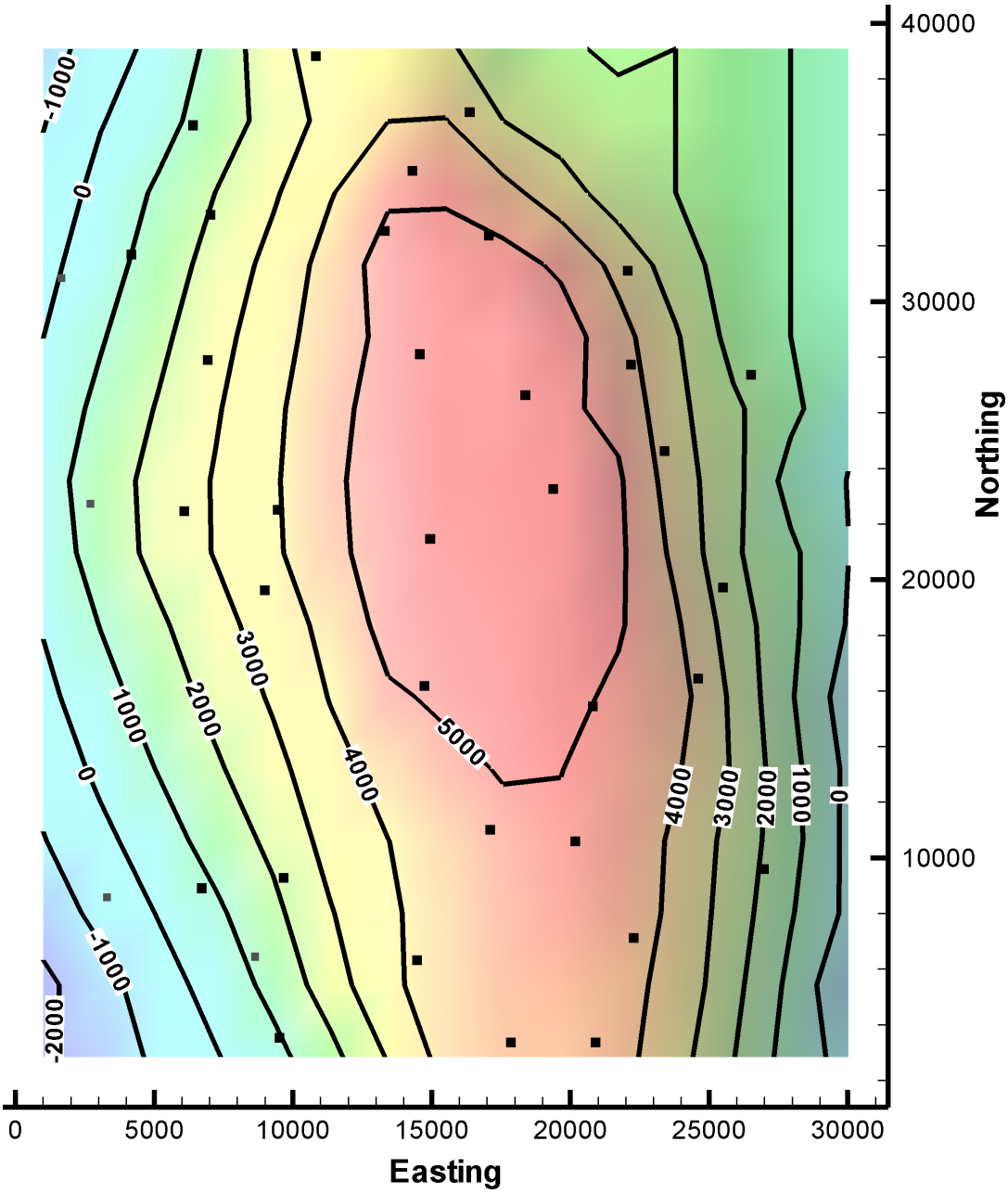

Fig. 3.29A. Composite structure contour map of the top Fairholme in the footwall of the thrust. All control points including wells are shown as *squares*. The coordinate system is in feet with arbitrary orientation and origin. Contours in feet

The angle $\rho = 10°$ and from Eq. 4.1 the true thickness is 73.9 m.

The data from the map in Fig. 4.19 are interpreted in Fig. 4.14. The same data are interpreted as isocore thicknesses in Fig. 4.16. Numerical data for this exercise are in text file "04-19dat.txt."

The tangent diagram of the data from Table 5.1 is shown in Fig. 5.8b.

The map in Fig. 6.53 is the same as in Fig. 7.17a,b, except that in Fig. 7.17 the fault is vertical.

The map in Fig. 6.54 is an enlargement of the graben and its borders from Fig. 6.14. The top marker in Fig. 6.14b is the one mapped in Fig. 6.54.

Figure 6.55 = Fig. 8.41b, rotated 90° counterclockwise.

Figure 6.56 = Fig. 8.46.

The section in Fig. 6.57 is complete in Fig. 6.16c.

The data for Fig. 6.58 are sampled from Fig. 6.25 which represents the circular-arc version of the cross section. A dip-domain interpretation is given in Fig. 6.58A.

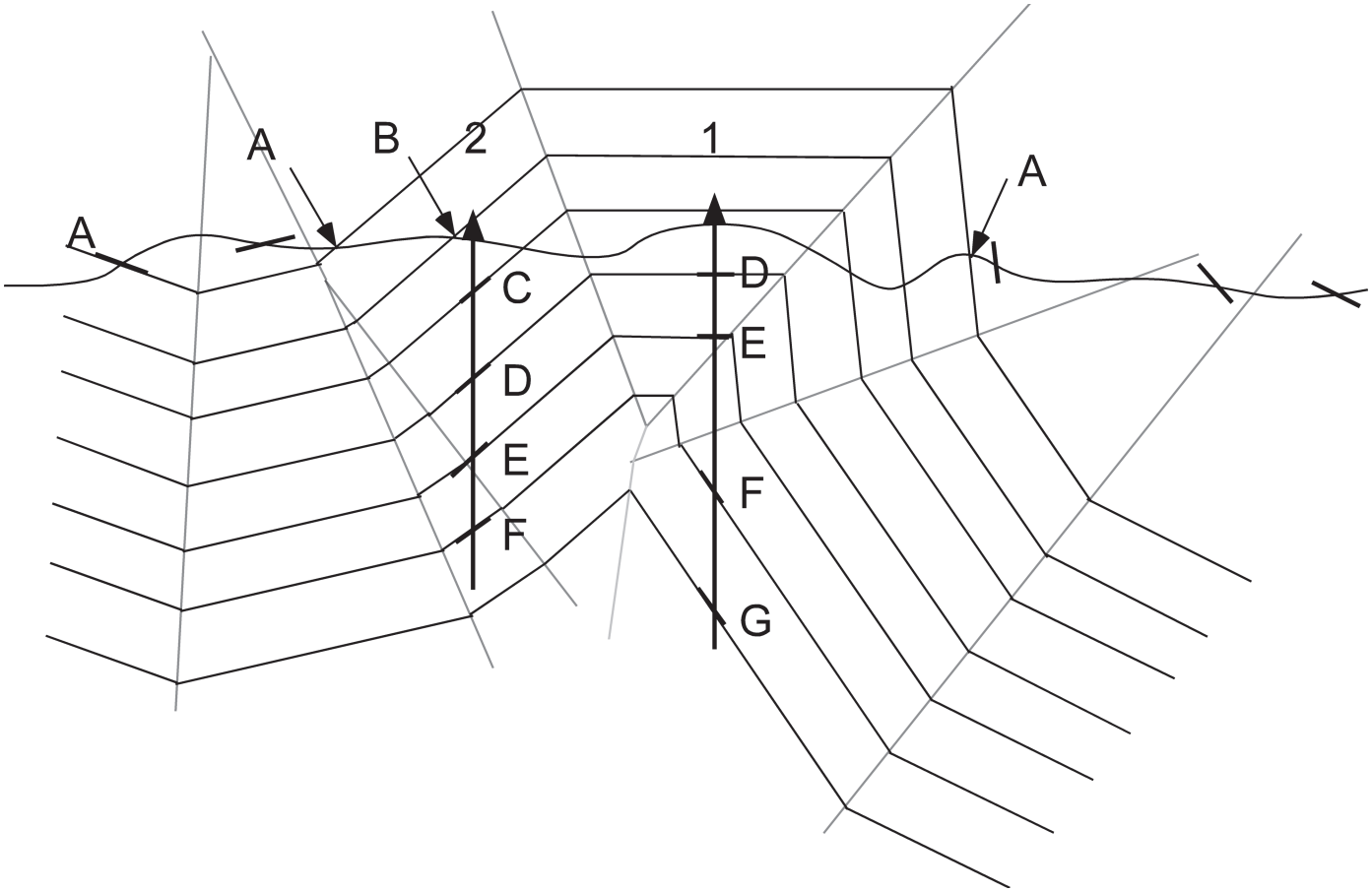

Fig. 6.58A. Dip-domain cross section of the Burma No. 1 and No. 2 wells by Marcella McIntyre

Project the well up plunge to the seismic line along the trend 045°. The elevation of the projected top is –962 m.

The interpreted version of Fig. 7.36 is Fig. 7.1. In addition, it would be reasonable to add a thrust fault separating the overturned lower Paleozoic of the Appalachian fold-thrust belt on the SE (C, D, E) from the upright, gently dipping upper Paleozoic of the Black Warrior foreland basin on the NW. All the faults of the Black Warrior basin (A) are normal faults. The normal faults probably terminate to the southeast at a bedding-parallel detachment.

The interpreted version of Fig. 7.37 is Fig. 7.2b.

The interpreted version of Fig. 7.38 is Fig. 7.4b. Beds with steep dips are not easily imaged on seismic reflection profiles and so the tight synclines and the tight anticline are not visible on the seismic line.

The faults are shown on Fig. 7.40A.

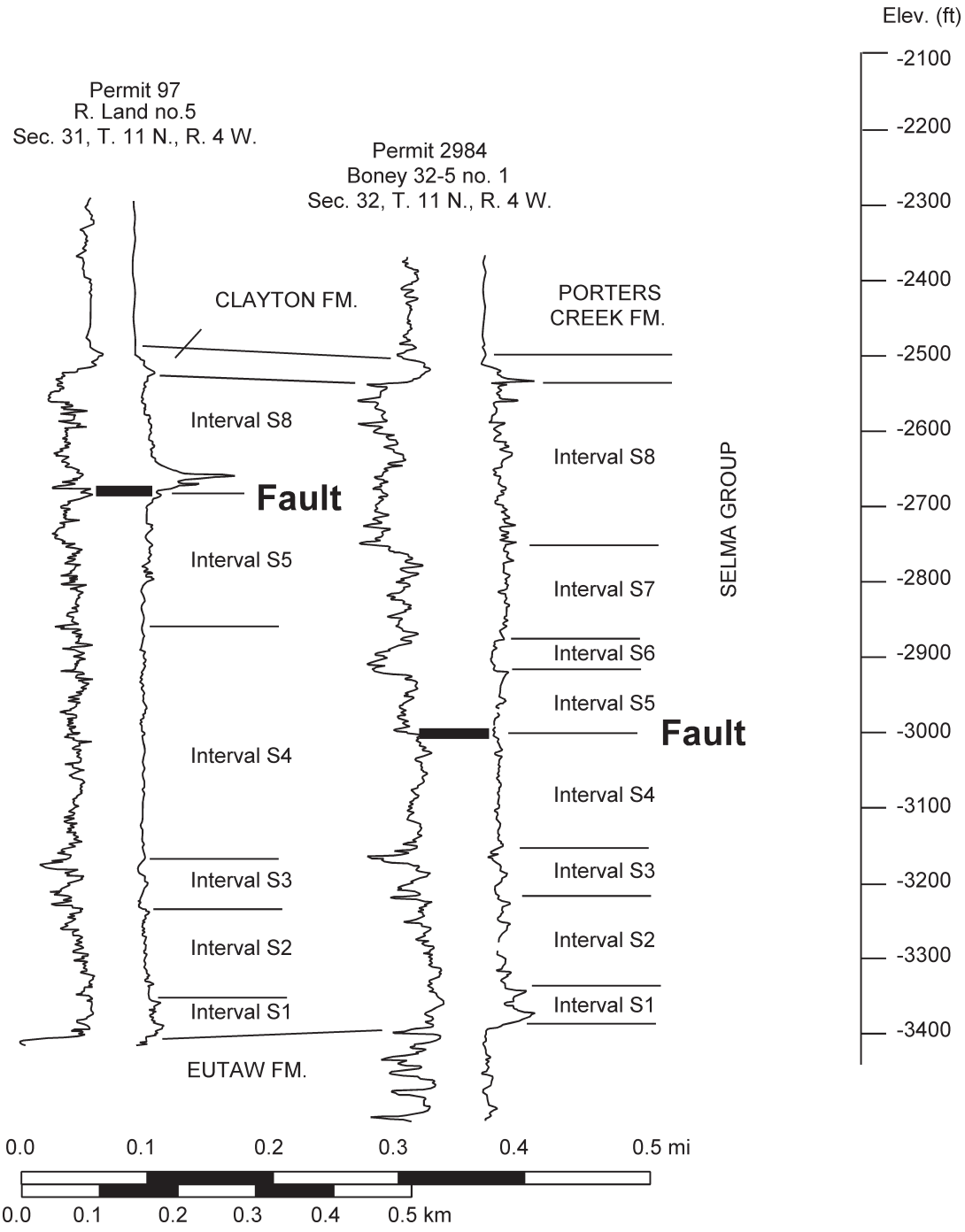

Fig. 7.40A. Interpreted logs of two faulted wells in Selma Chalk (after Pashin et al. 2000)

Faulted wells 2, 3, and 4 belong to one fault, and well 1 belongs to another. The critical evidence is the lack of a fault cut in the well just SW of a line between wells 1 and 4: it should pass through the fault plane but does not have a fault cut. Additionally, the fault through wells 2, 3 and 4 is parallel to a structural trend on the marker horizon that could represent the footwall of the fault.

Table 7.2A contains the answers.

Table 7.2A. Fault attitude and separation data

Fault attitude	Stratigraphic separation	HW attitude	FW attitude	Fault cut in	ρ	Heave	Throw	Vertical separation
60, 270	100	0	0		30	57.7	100	100
60, 270	100	20, 070	30, 200[a]	HW	48	74.7	129.4	115.5
		20, 070[a]	30, 200	FW	13	51.3	88.9	106.4
30, 200	100	0	0		49	173.2	100	100
30, 200	100	20, 070	30, 070[a]	HW	45	121.8	70.3	115.5
		20, 070[a]	30, 070	FW	49	131.2	75.8	106.4

[a] Cross-fault bedding attitude.

The heave is 25 m and the throw is 70 m.

The interpreted maps are shown in Fig. 8.50A.

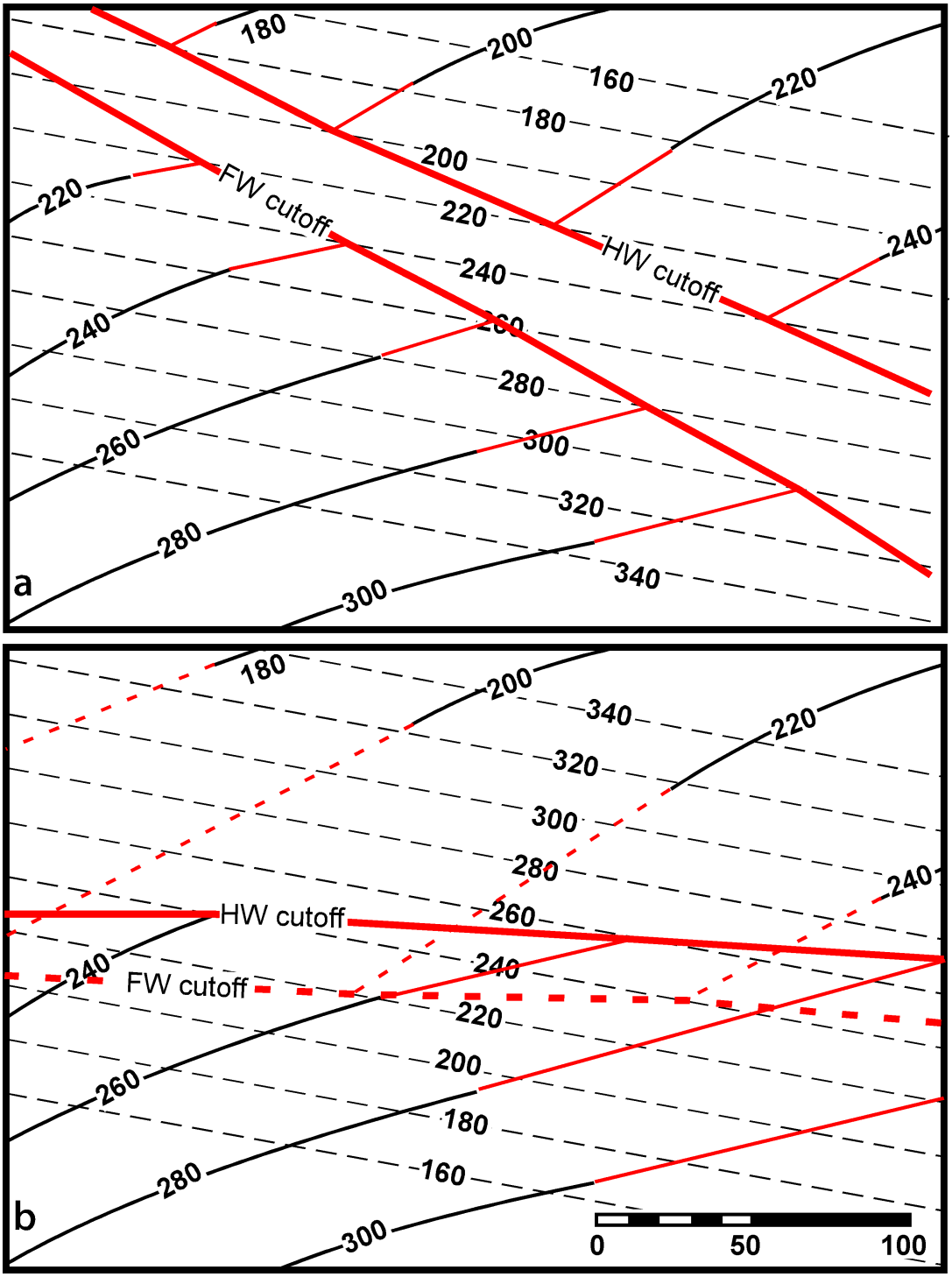

Fig. 8.50A.
Interpretation of Fig. 8.50, fault plane dashed. **a** Normal fault. **b** Reverse fault. *HW: solid lines; FW: dashed lines*

The interpreted map is in Fig. 8.52A. Numerical data for this exercise are in text file "08-52dat.txt."

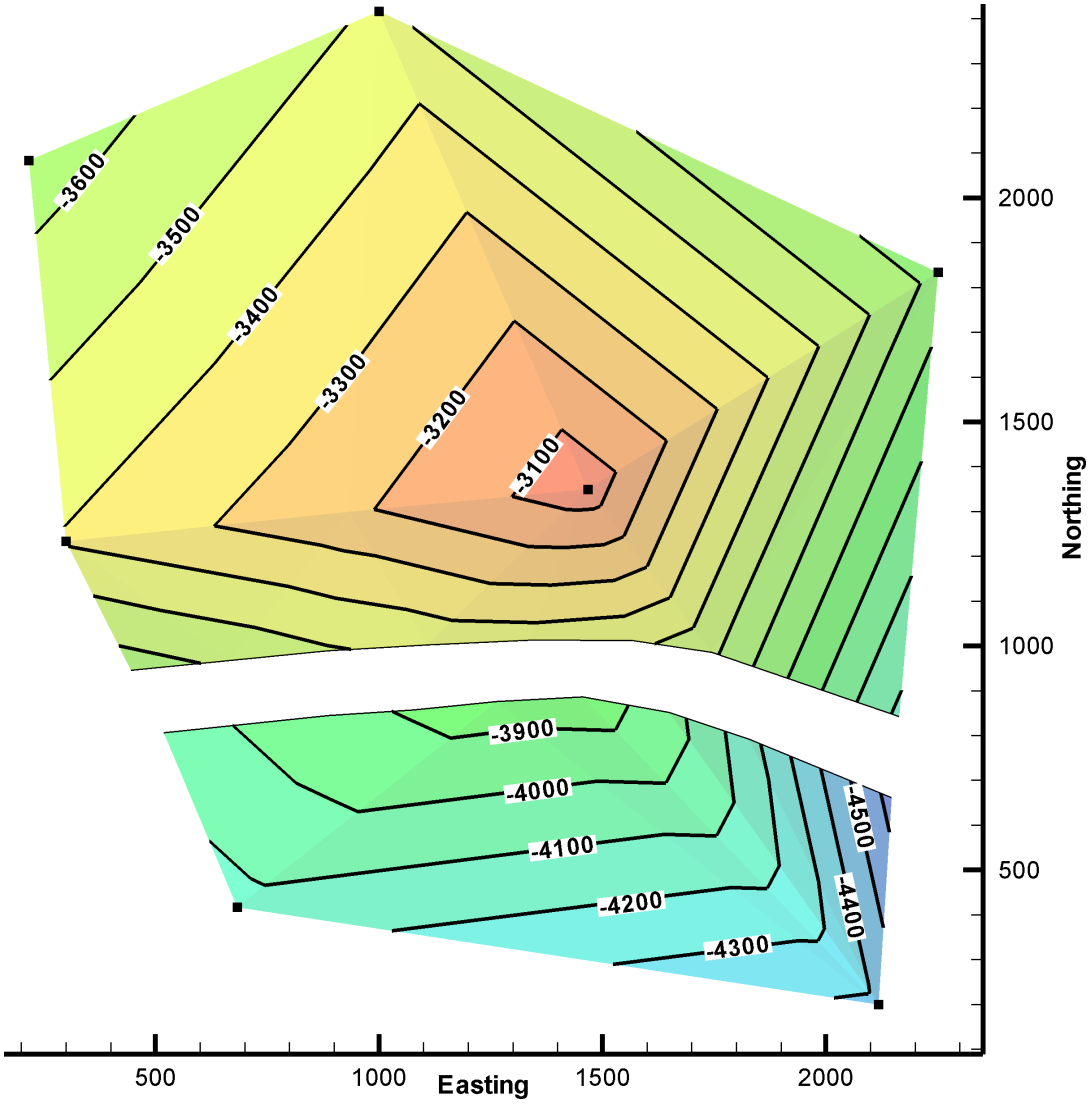

Fig. 8.52A. Interpreted map on the top Hamner Sandstone reservoir. The fault dips about 70° south and has a constant throw of 500 m

The interpreted map is in Fig. 8.53A. Numerical data for this exercise are in text file "08-53dat.txt."

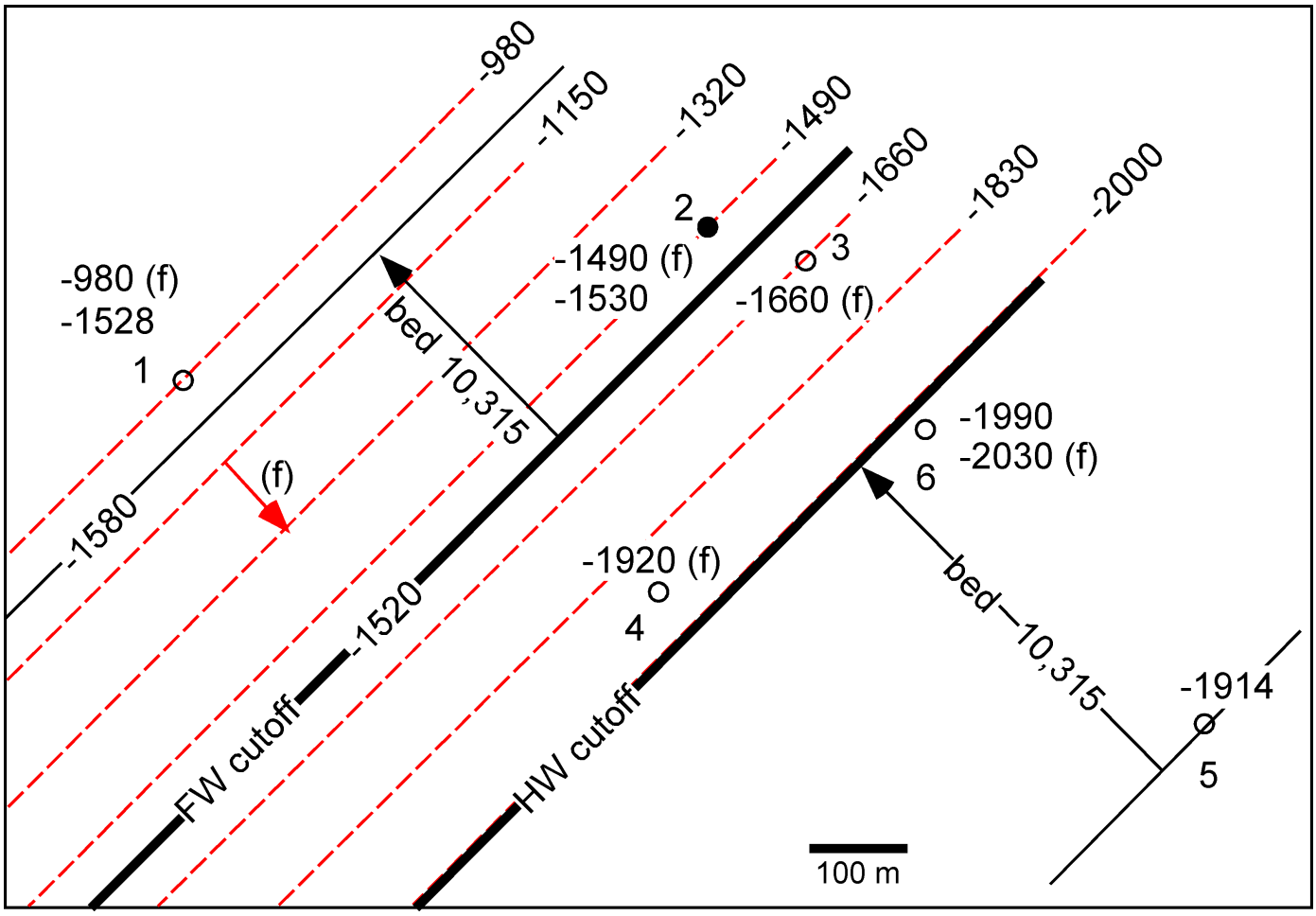

Fig. 8.53A. Interpreted faulted top of Oil City sandstone. Fault contours are *dashed*. The oil is in a footwall uplift trapped against the fault

The fault dips about 45° E and has a reverse separation. The footwall shale marker dips gently to the NW. A spill of heavy liquid in the stream valley would sink vertically until it reached the shale, then migrate down the footwall dip to the NW. The footwall cutoff of the fault is up dip to the SE and would have no effect on the migration of a heavy liquid. Numerical data for this exercise are in text file "08-54dat.txt."

The map in this exercise is interpreted in Fig. 8.26. The major thickness changes on the map are the result of missing section caused by normal faults. Note that the unit does not maintain *exactly* constant thickness because the faults are growth faults.

The fault cutoff map in this exercise is the America seam, interpreted in Fig. 8.18. The vertical exaggeration is greater in the exercise to make the construction easier. Note that footwall elevations toward the NW end of the fault zone are those of the small overlapping fault.

The cutoff map is in Fig. 8.57A.

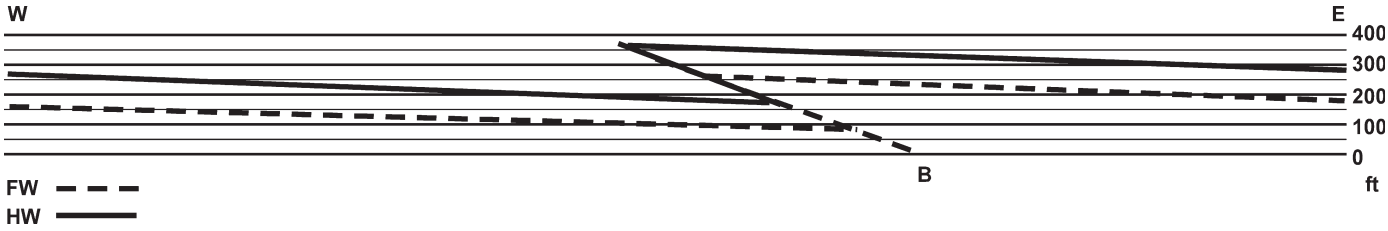

Fig. 8.57A. Cutoff map of the marker horizon on fault A, view to N, projected onto a vertical plane. No vertical exaggeration

The relay zone in the Northriver Sandstone is mapped in Fig. 8.59A. The data define the fault planes fairly well, assuming they are planes. The exact geometry of the upthrown and downthrown blocks and the ramp could differ from this map and still agree with the data. Numerical data for this exercise are in text file "08-59dat.txt."

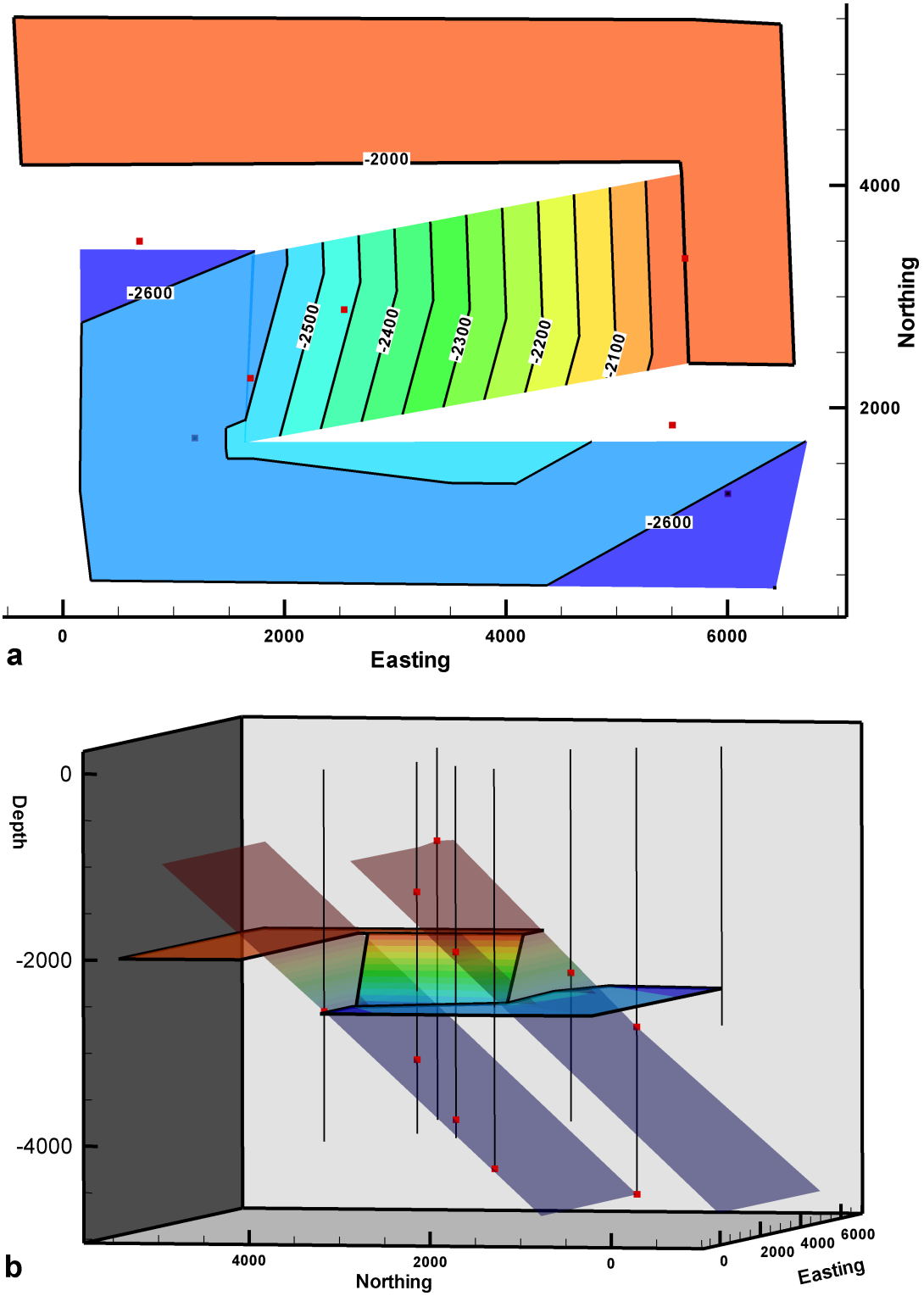

Fig. 8.59A. Interpreted top of Northriver Sandstone. **a** Structure contour map. **b** 3-D interpretation showing fault planes and wells. Fault cuts in wells are *red squares*

The interpreted map is in Fig. 8-60A. The geometry is a branching fault. Numerical data for this exercise are in text file "08-60dat.txt."

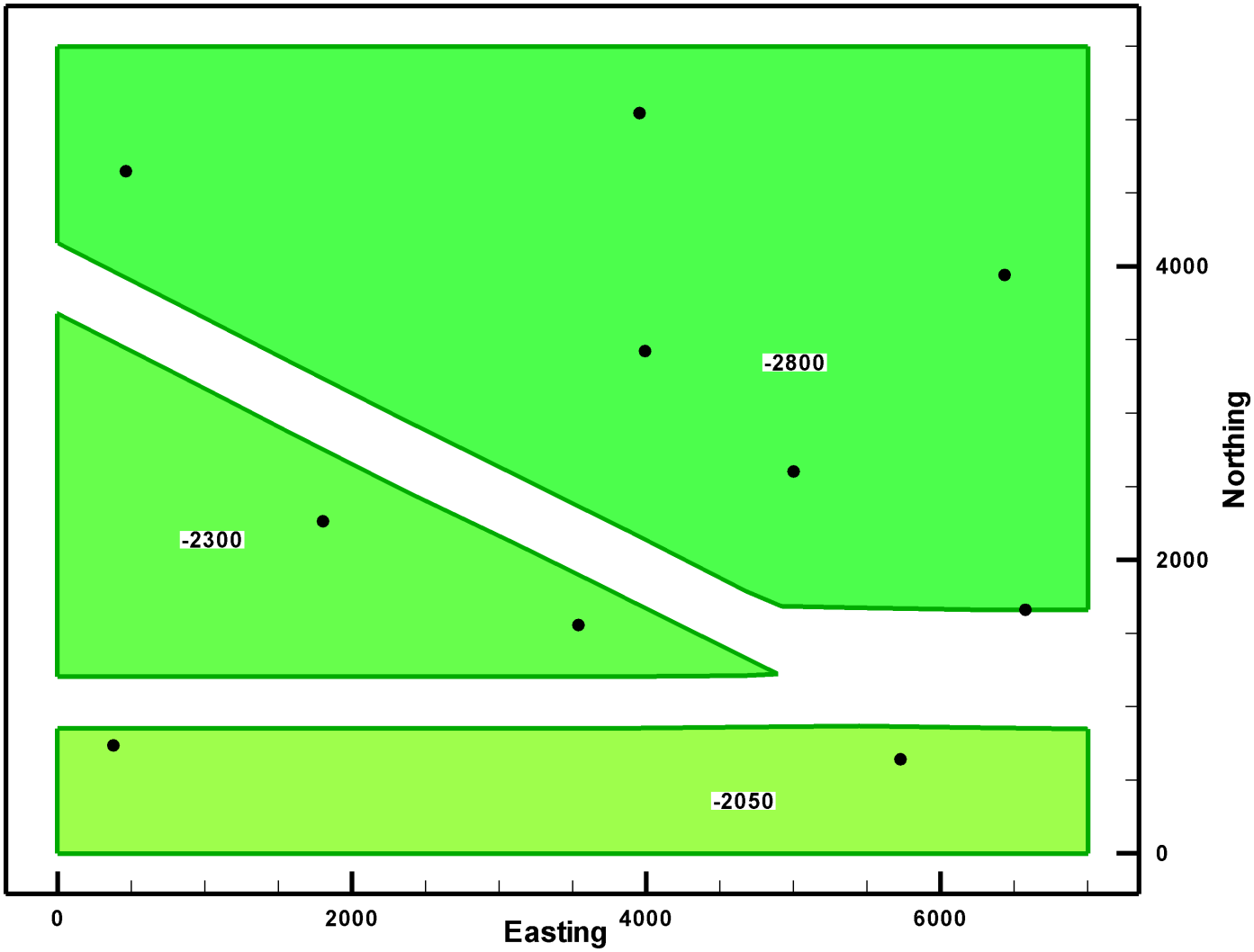

Fig. 8-60A. Interpreted top of Reef Limestone. Each fault block has been interpreted to be horizontal

The interpreted map of a splaying fault is in Fig. 8.61A. Numerical data for this exercise are in text file "08-61dat.txt."

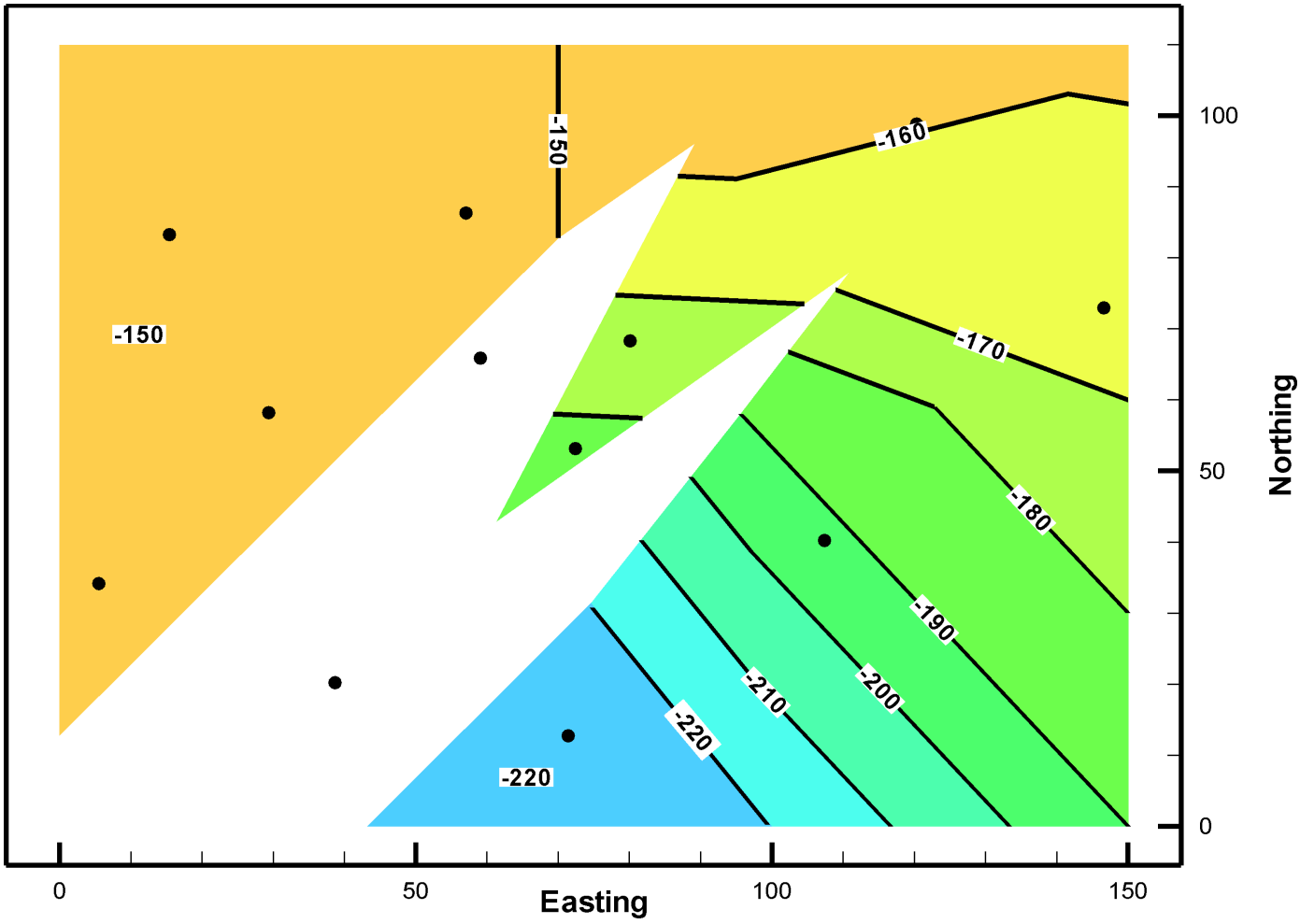

Fig. 8.61A. Top of clay seam. The footwall block is nearly horizontal

The interpreted map is in Fig. 8.62A. The fault block containing the oil well was not closed until the second (*blue*) fault formed. Numerical data for this exercise are in text file "08-62dat.txt."

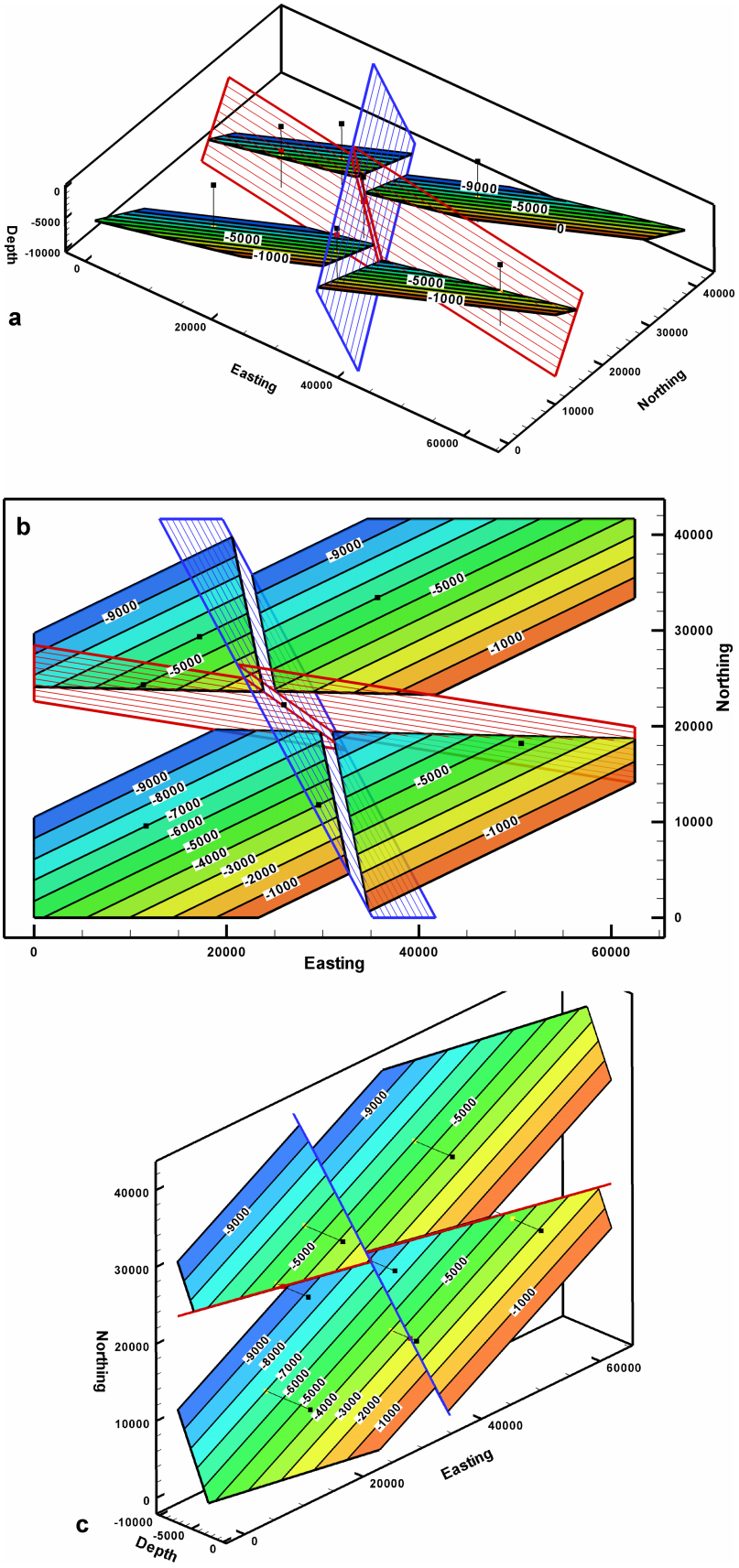

Fig. 8.62A. Interpreted map of the top of the A sand (*solid colors*). **a** Oblique view to NW. **b** Plan view. Faults indicated by *unshaded red* and *blue contours*. Wells shown by *black squares* and *lines*. **c** View downward along line of intersection of the two faults showing the red fault offset on the blue fault

The interpreted map is in Fig. 8.63A. The red fault is offset by the blue fault. There was no closure until after the blue fault formed. Numerical data for this exercise are in text file "08-63dat.txt."

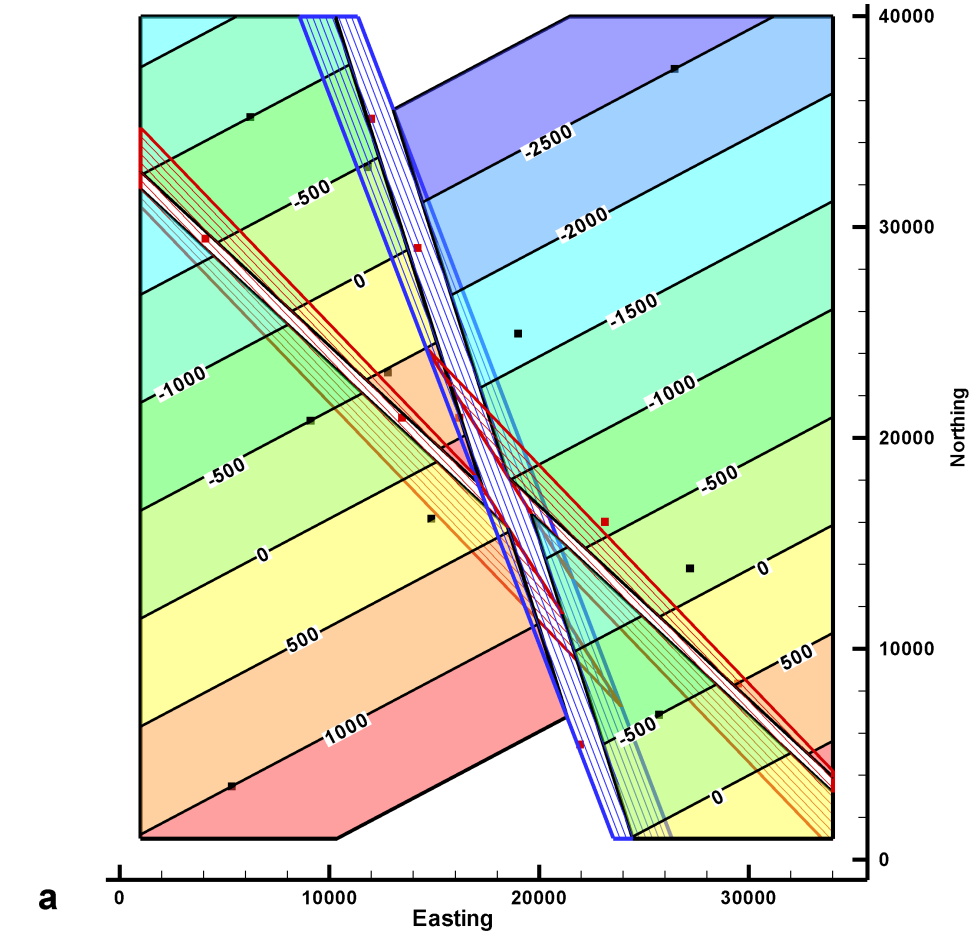

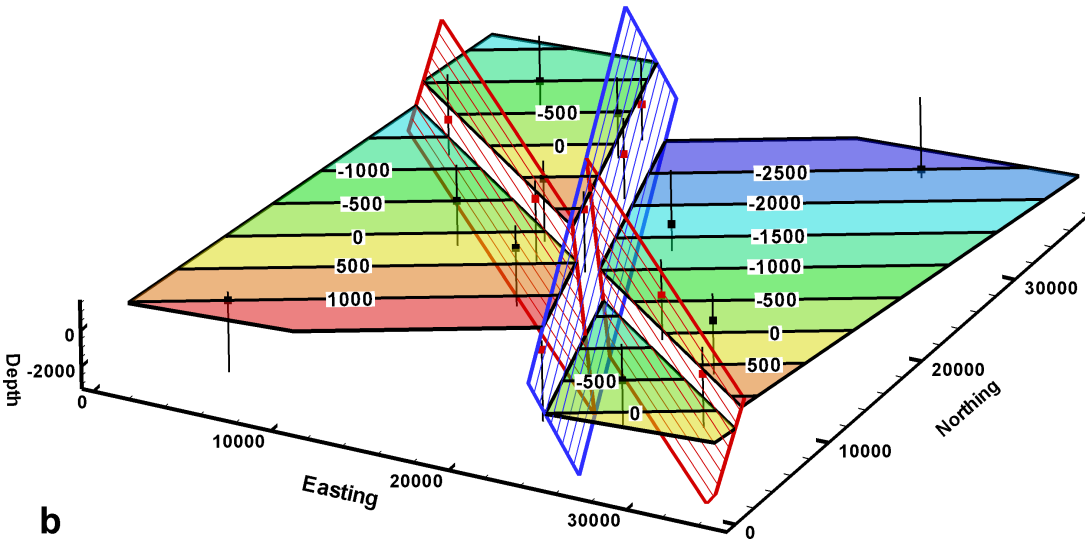

Fig. 8.63A.
Top of the Northport Dolomite. Top dolomite: *black squares* and *shaded contours*; fault cuts: *red squares*. Fault planes are *contoured* but *unshaded*. **a** Plan view. **b** Oblique view to NW

The Sequatchie anticline is interpreted in the text, Figs. 9.14 to 9.16.

This example is on the northwest dipping forelimb of the major Greasy Cove-Wills Valley anticline in the southern Appalachian fold-thrust belt. The regional dip of the forelimb of around 30° northwest is seen outside the map area. On the azimuth-dip diagram (Fig. 9.26A1), the dips from the map area show a vertical scatter trend along the dip direction of the forelimb, as expected for a fault parallel to regional strike. The T direction is 310 and the L direction is 220. The dip components are determined from the T and L directions (Table 9.3A). ▸

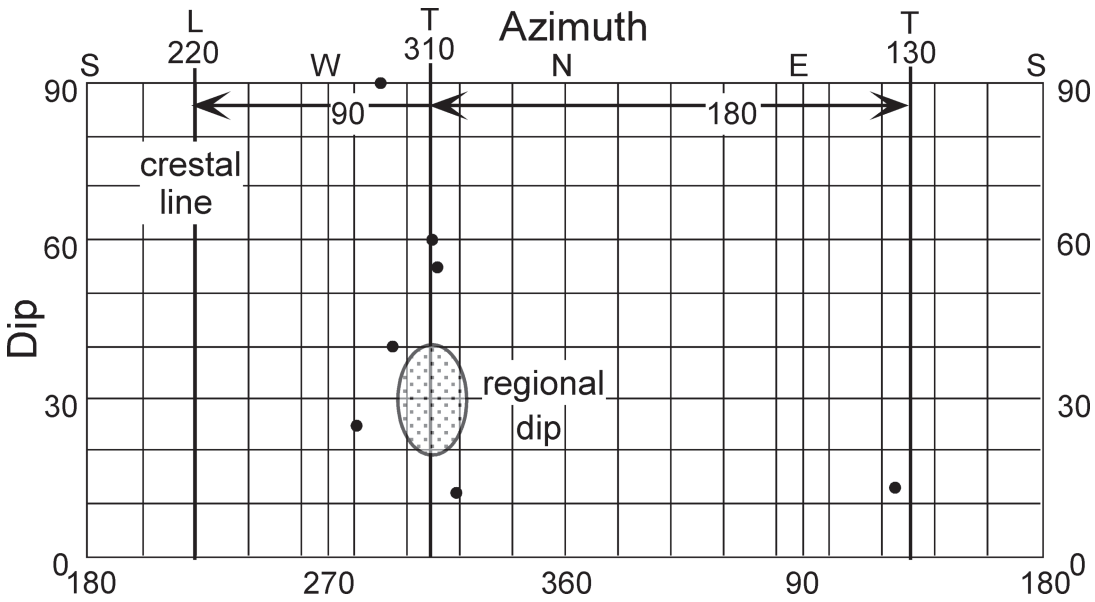

Fig. 9.26A1. Dip-Azimuth diagram for the Bald Hill map area

Table 9.3A. Dip traverse data from the Bald Hill map area. Dips of 90° are at infinity on the tangent diagram

Distance from the northwest (km)	Attitude Dip, azimuth	T component	L component
0.54	60, 310	60 NW	0
0.70	90, 289	NW	SW
0.90	55, 311	55 NW	2 NE
1.10	40, 295	38 NW	12 SW
1.30	14, 124	13 SE	4 NE
2.38	12, 319	12 NW	3 NE
2.68	26, 281	23 NW	15 SW

The azimuth distance diagram (Fig. 9.26A2a) shows the regional northwesterly dip with one aberrant point that dips to the southeast. The dip-distance diagram (Fig. 9.26A2b) shows a high degree of scatter that does not suggest any interpretation. The component plots significantly clarify the interpretation. Dips over about 80° are not practical to break into components because of their extreme magnitude, and so the 90° dip is shown on the component plots as an open circle at the edge of the diagrams. The T component plot (Fig. 9.26A2c) suggests the cusp pattern of a fault, with the fault being close to the fourth point (40, 295). The L component plot (Fig. 9.26A2d) shows moderate scatter around zero, indicating that the direction of the plunge was chosen correctly. The map as originally given by Burchard and Andrews (Fig. 9.26A3) shows a fault between dip measurements 4 and 5, in the predicted location. This fault runs nearly parallel to bedding and neither removes nor repeats a formation boundary. ▸

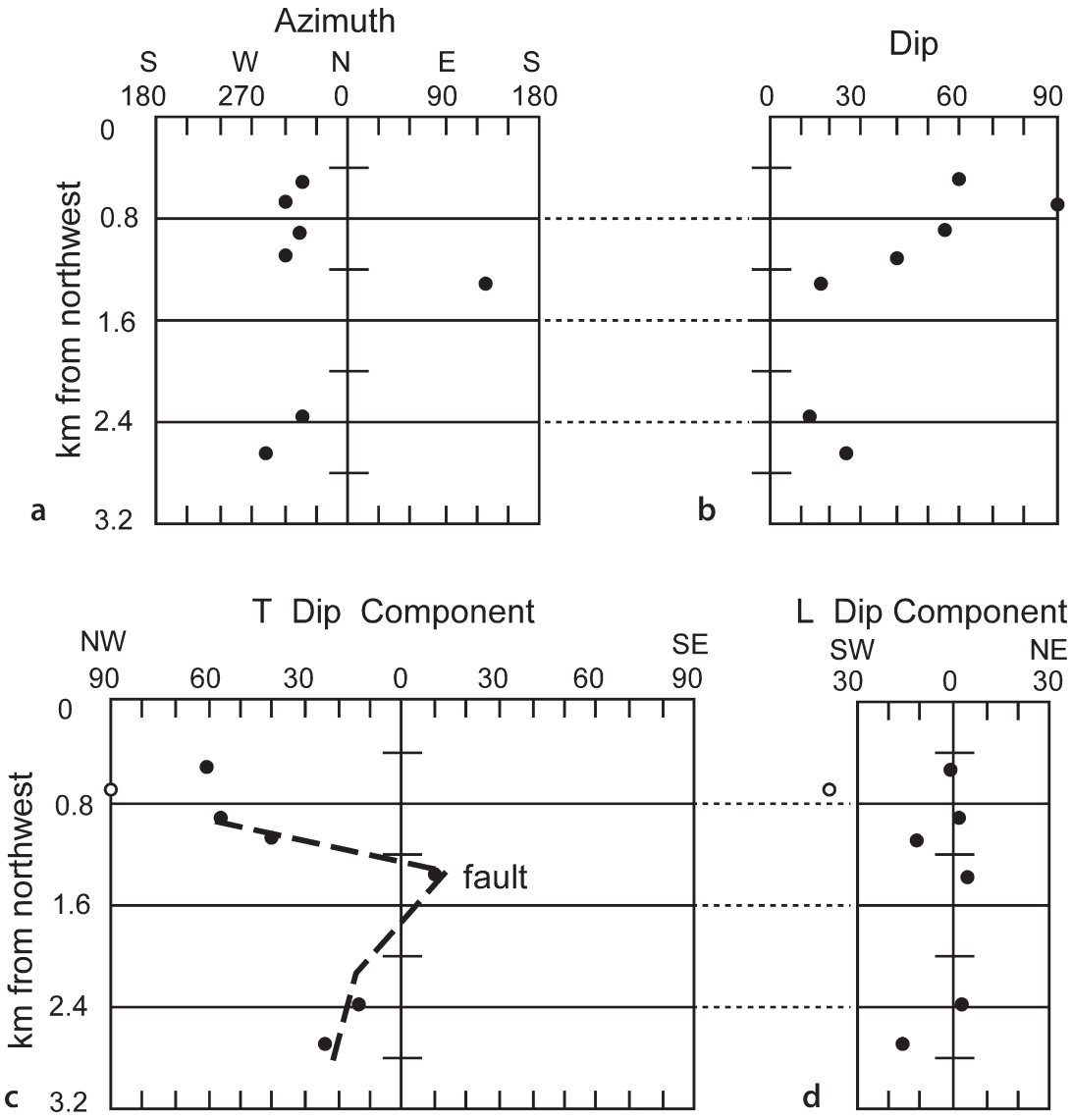

Fig. 9.26A2. Dip sequence analysis of a portion of the Greasy Cove anticline. **a** Azimuth-distance diagram. **b** Dip-distance diagram. **c** T component dip-distance diagram. *Open circle* is the 90° dip which plots off scale. **d** L component dip-distance diagram. *Open circle* is the 90° dip which plots off scale

From the dip sequence analysis alone, the fault could be either normal or reverse. If the fault is normal it should dip in the direction that the cusp points on the T component plot, that is, to the southeast. If the fault is reverse, it should dip to the northwest, opposite to the direction of the cusp. Which is the more reasonable interpretation?

The best choice of the fault dip direction and sense of separation can be inferred from the local structural style. The first-order structure in the Bald Hill area is an anticline produced by northwest-southeast horizontal compression. A large reverse fault crops out in the forelimb of the anticline to the northeast along strike. This reverse fault dips to the southeast, as is usual for the major thrusts in the forelimbs of Appalachian folds. A preliminary hypothesis might be that the fault at Bald Hill is also a southeastward dipping reverse fault. The dip traverse analysis indicates, however, that the fault cannot both be southeastward dipping and have a reverse separation. If the dip is to the southeast, it should be a normal fault. Normal faults parallel to the strike are virtually unknown in Appalachian folds whereas second-order conjugate thrusts are relatively common. Thus, the favored interpretation would be that the fault is reverse and, from the dip traverse analysis, dips to the northwest (Fig. 9.26A4). Along strike to the southwest from the map area in Fig. 9.26A3, both the bedding and the fault dip to the northwest where they "V" across a valley, in agreement with the interpretation of Fig. 9.26A4.

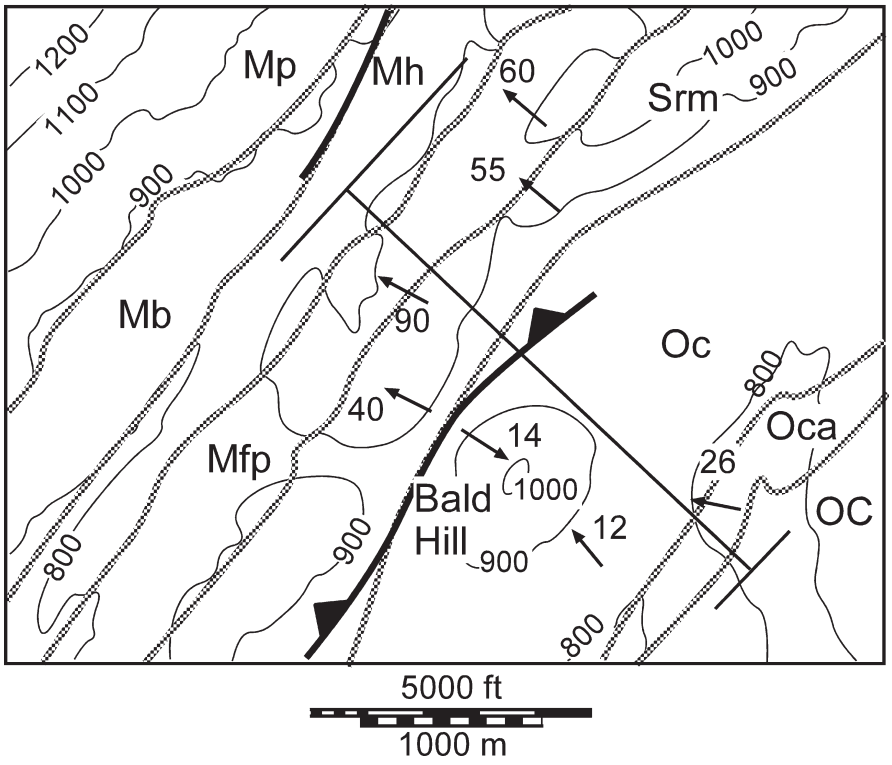

Fig. 9.26A3. Geologic map of the Bald Hill area. Topographic contours (in feet) are *thin lines*; geologic contacts are *wide gray lines*; faults are *heavy solid lines*. The fault at Bald Hill is interpreted to be a thrust that dips to the northwest. (After Burchard and Andrews 1947)

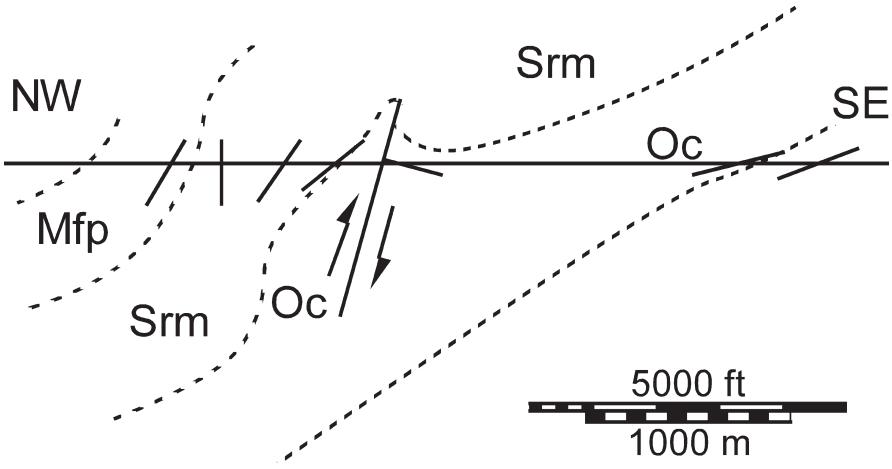

Fig. 9.26A4. Speculative cross section along the dip traverse across Bald Hill showing the T component dips and the inferred fault. The fault dip amount and separation are unknown

The cross section in Fig. 10.27 is interpreted correctly in Fig. 6.34c and confirmed by mapping the fault in Fig. 6.44. The projection technique used to create Fig. 10.27 is inappropriate.

The implied fault surfaces in the map (Fig. 10.28) range from unlikely to impossible. The fault surfaces are constructed in Fig. 10.28A by joining the HW and FW cutoff lines across the faults. Fig. 10.28Aa shows that the NE-trending fault changes its dip direction along strike. This is unlikely unless it is a wrench fault. Fig. 10.28Ab shows that the NW-trending fault has a continuous spiral shape, an impossibility. Assuming that all the control data are correct, the area could be remapped with a single, approximately EW-trending normal fault that interrupts a generally northward-dipping limestone bed. Numerical data for this exercise are in text file "10-28dat.txt."

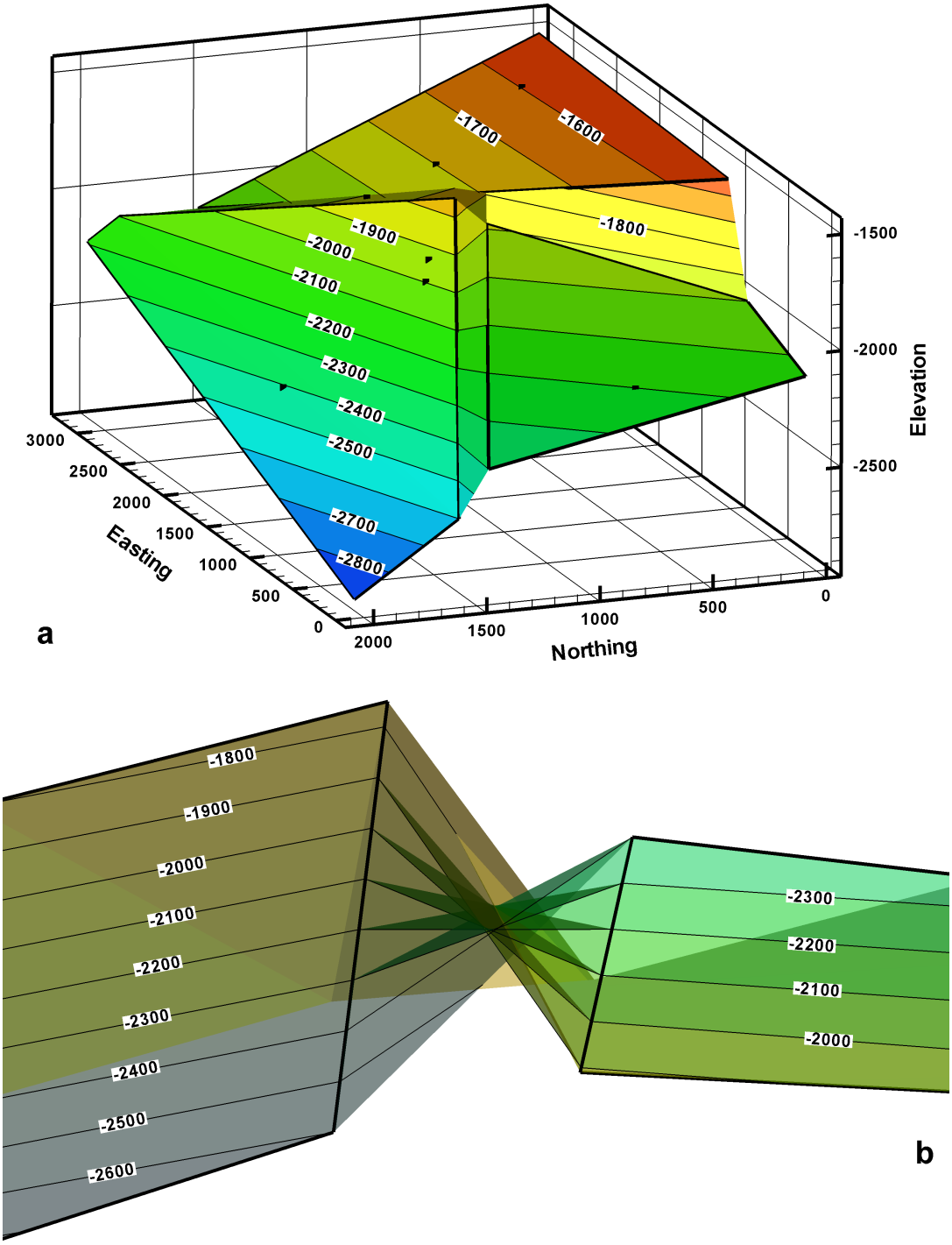

Fig. 10.28A.
3-D views of map implied by Fig. 10.28, constructed with plane surfaces. **a** Oblique view to E. *Black squares* are well locations. **b** View NW parallel to NW-trending, spiral-shaped fault

The vertical separation at the well location is about 14 m and the stratigraphic separation is 12 m.

The cross section in Fig. 11.65 is area balanced based on its area-depth graph (Fig. 11.65A). The lower detachment is at –8.5 km below sea level and the displacement that formed the structure is 3.04 km. The predicted strain in each layer is 1 = –8.0%; 2 = –18.6%; 3 = –26.0%, calculated from Eq. 11.26. Strains of these magnitudes would imply substantial sub-resolution faulting in low temperature deformation.

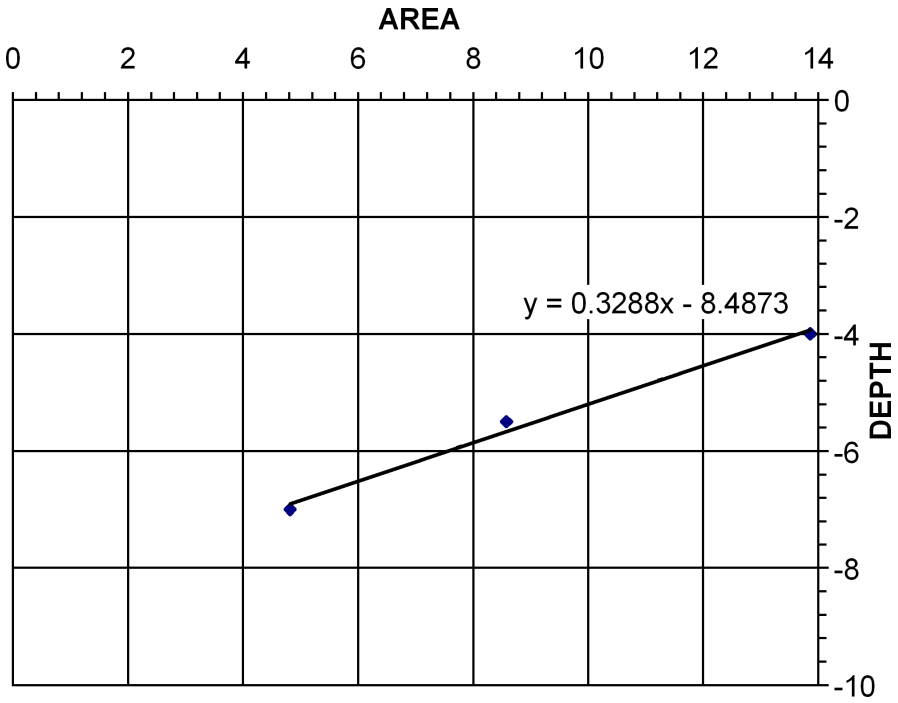

Fig. 11.65A.
Area-depth graph for the detachment fold in Fig. 11.65. Depth in km, area in km^2

The cross section in Fig. 11.66 is area balanced, based on the linear area-depth relationship (Fig. 11.66A). The lower detachment is at –3451.5 ft below sea level and the displacement that formed the graben is 262.3 ft. This is the same structure described in Fig. 11.21 with a different reference level. The predicted strain in each layer is 1 = –1.6%; 2 = –1.4%; 3 = 0.6%; 4 = 11.8%; 5 = 32.8%; 6 = 36.1%; 7 = 40.3%. The small strain magnitudes inferred for layers 1–3 probably represent the magnitude of the uncertainty associated with the measurements. The large values of extension calculated for layers 4–7 indicate significant sub-resolution deformation. The deeper layers in the graben almost certainly contain additional sub-resolution normal faults.

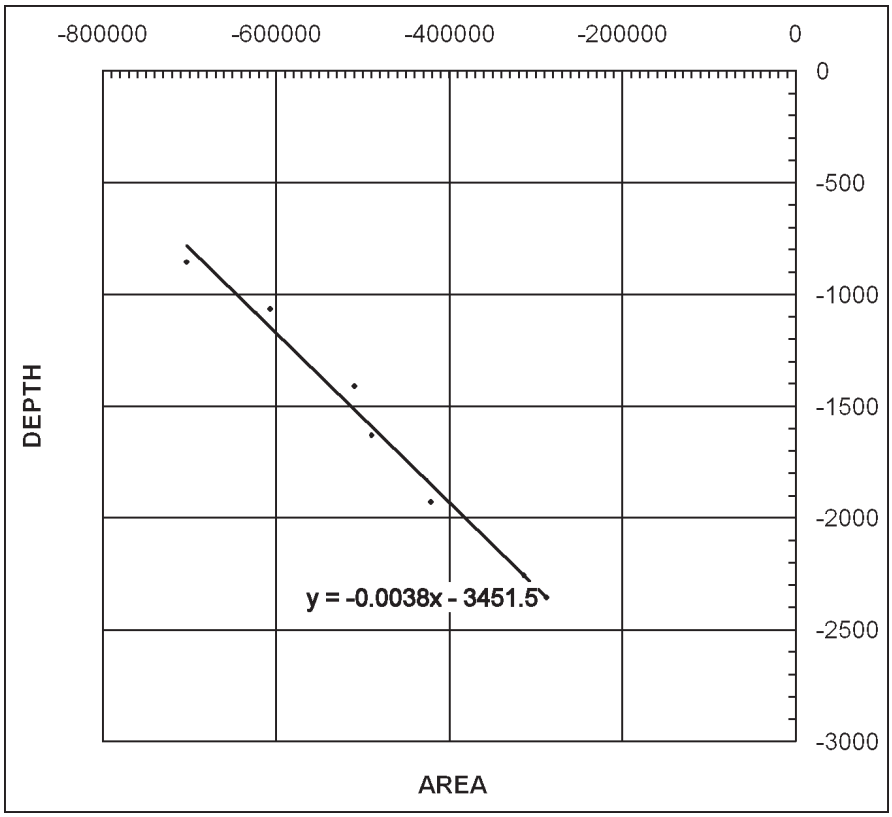

Fig. 11.66A. Area-depth graph for the full graben in Fig. 11.66. Depth in ft, area in ft^2

All three cross sections in Fig. 11.67 restore perfectly. The cross sections represent the cross cutting conjugate faults illustrated in Figs. 8.40, 8.44, and 8.47.

The Rhine Graben cross section in Fig. 11.68 is appropriately restored with rigid-block displacement. The sequential restoration is shown in Fig. 11.9. The cross section is valid.

The Sequatchie anticline (Fig. 11.69, from the example in Fig. 6.23) is a compressional fold for which flexural-slip restoration is appropriate. The best choice of pin line and loose line would be where the structure returns to regional dip. As this does not occur on the cross section, a small uncertainty is introduced into the result. Vertical pin and loose lines or bed-normal pin and loose lines are both reasonable choices. Regardless of the choice, the restoration (Fig. 11.69A) is short of bed length in the deeper beds. It is likely that one or more small faults repeat bedding deep in the structure.

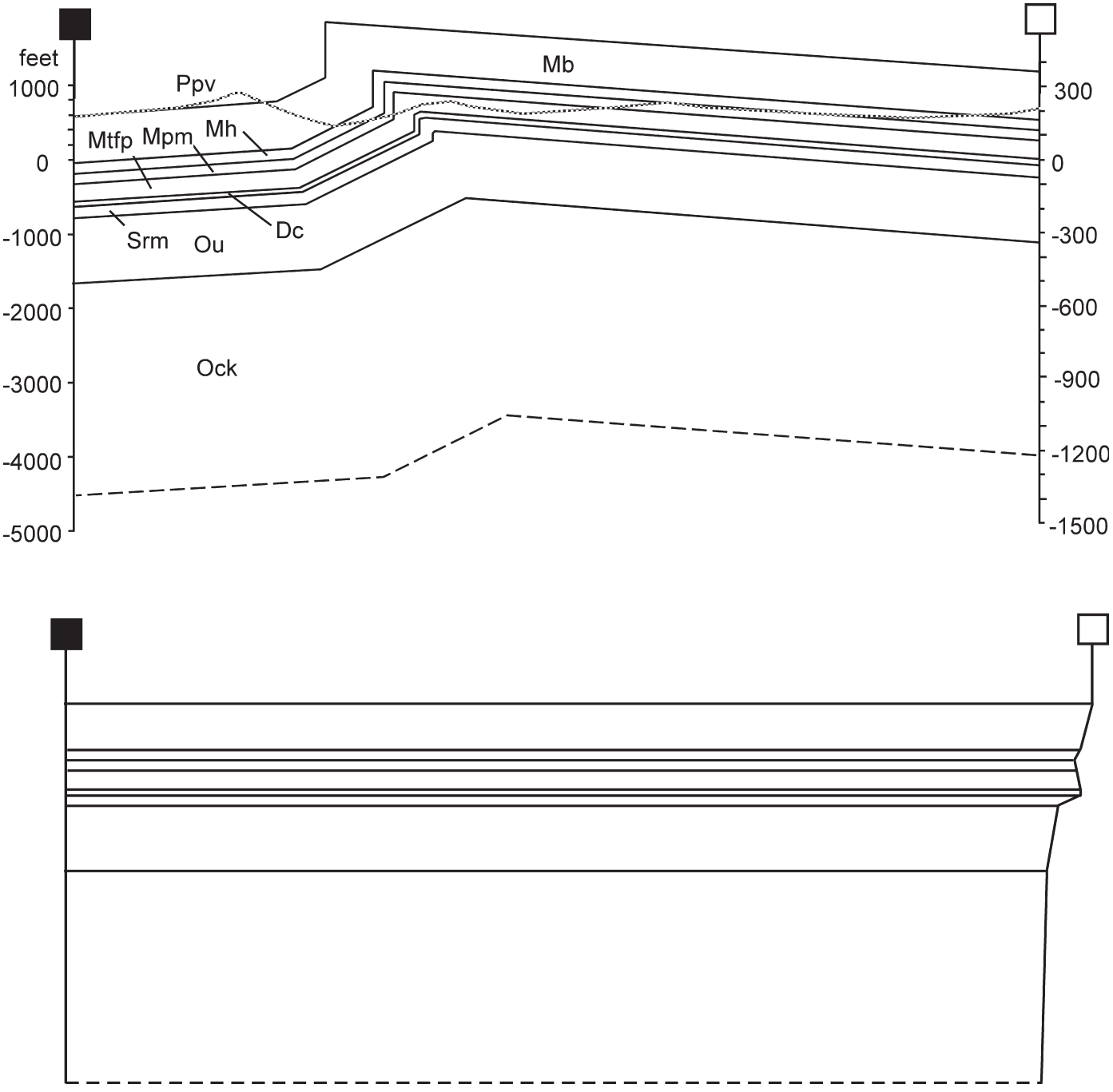

Fig. 11.69A. Flexural-slip restoration of the Sequatchie anticline

The cross section through the Velma area (Fig. 11.70) is discussed at the end of Sect. 11.6.1 and is restored in Fig. 11.35b.

The units on the cross section from the Rhur basin (Fig. 11.71) are correlated and restored in Fig. 11.71A. The seismic profile along this line (Fig. 7.4a) could be interpreted in numerous ways and so it is reasonable to question the validity of the cross section. The pin line is placed normal to bedding in the least deformed part of the section. The loose line is placed along the axial trace of the right-side anticline. In order to have a more complete restoration, the anticline has been continued above the unconformity as a circular-arc style fold. The restoration of the loose line is fairly good in all but the uppermost bed. Because a considerable portion of the uppermost bed has been inferred, its lack of bed length is not very significant. Thus it can be concluded that the section is reasonably well balanced and therefore valid.

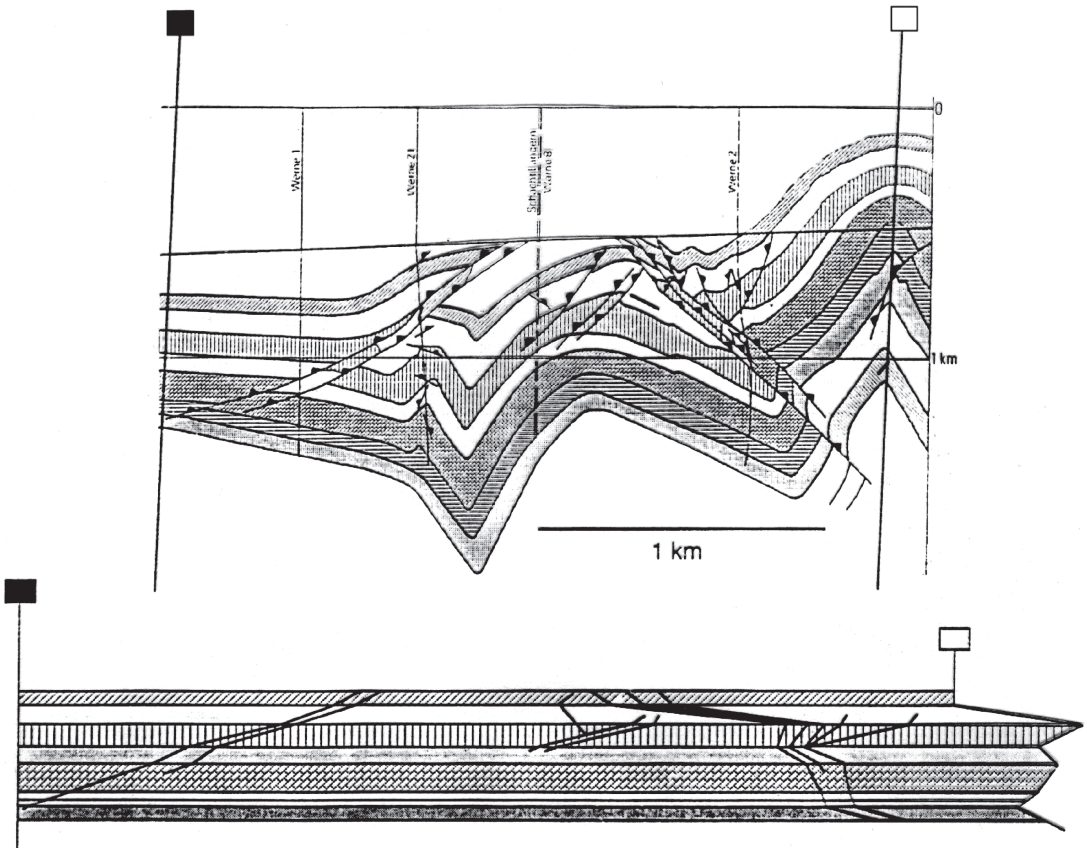

Fig. 11.71A.
Flexural-slip restoration of the Rhur cross section by Jerry Bowling

The cross section in Fig. 11.72 is locally balanced, based on the area-depth line (Fig. 11.72Aa). Note that the section has a sloping regional and so depth measurements are taken from the center of the structure (Fig. 11.72c). The predicted lower detachment is 0.2 km shallower than shown on the original interpretation (Fig. 11.72Aa,c), which is a significant difference. Examination of the seismic line on which the cross section is based suggests that the detachment is properly located. The possible changes that could produce better agreement illustrate the issues that must be considered in validating an interpretation. A change in the position of area-depth point T would produce a better match. Realistic changes in the depth to the regional of marker T are about ±0.1 km and will not produce much change in the predicted detachment depth, which means that the probable change is an increase in the excess area under marker T. The area of T could be increased by either changing the interpretation of the cross section or by lowering the position of the regional. The regional (Fig. 11.72Ac) seems consistent with the structure and so should probably not be changed. The T marker is below the regional at two locations. Reinterpreting the section to place the T marker entirely above the regional would increase the excess area by 0.16 km^2, also insufficient by itself to place point T onto the dashed line on the area-depth graph. The interval between marker 2 and T is greater in the duplex than outside it. A reinterpretation of the location of T to keep the interval constant (*red* in Fig. 11.72Ac) increases the excess area enough to place the predicted detachment slightly below the interpreted detachment (Fig. 11.72Ab,c). Thus if it is possible to change the geological interpretation, reinterpreting the position of the Trenton limestone is the most reasonable aspect to change.

Another aspect of the interpretation is the predicted strain. Based on the reinterpreted location of the Trenton, the requisite strains are T = –1.6%, 2 = –16.3%, 3 = –12.2%, 4 = –13.3%. The small value for the Trenton represents essentially constant bed length. The larger values for the shallower markers indicate significant sub-resolution layer-parallel shortening should be present, presumably in the form of small faults or folds. Bed length restoration of the cross section, as given, would falsely indicate insufficient bed length in the upper units.

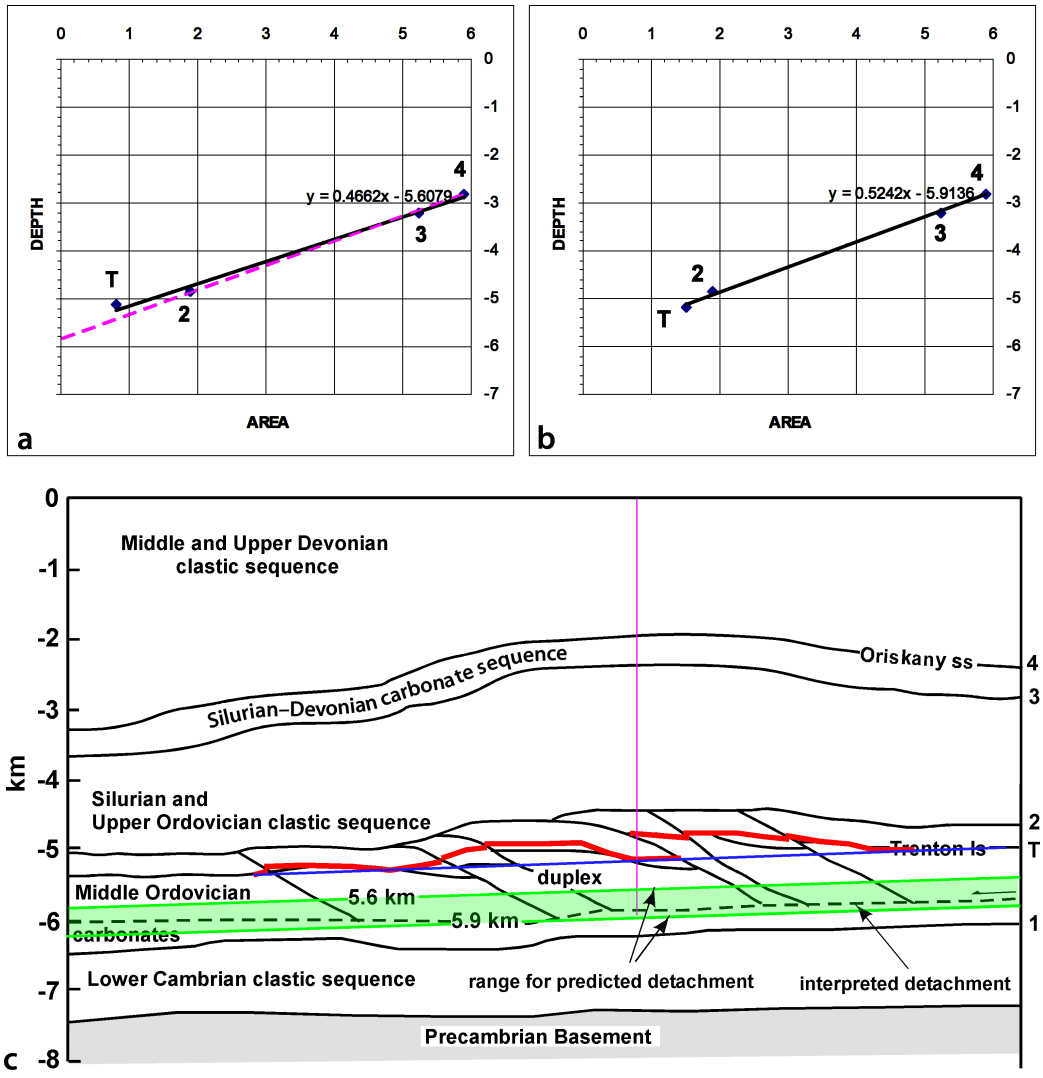

Fig. 11.72A. Area-depth interpretation of Deer Park anticline (from Fig. 11.72). **a** Area-depth graph in km^2 and km, respectively. *Heavy line* is least-squares best fit giving a predicted lower detachment at –5.6 km. *Thin dashed line* is drawn to intersect lower detachment at –5.8 km. **b** Revised area-depth graph based on reinterpretation of excess area of T, giving lower detachment at –5.9 km. **c** Cross section showing predicted and interpreted detachment levels. The Trenton (T) regional is *blue*; reinterpreted Trenton marker is *red*, predicted detachment levels are *green*; the *vertical purple line* is the location of depth measurements

A rotated-block model is fit to the cross section of the South Hewett fault zone in Fig. 11.73A. The most important assumption is that the original seismic line was displayed with approximately zero vertical exaggeration. A change in the vertical scale would change the numbers but should not change the form of the interpretation. The result depends on the correct choice of the regional and the resulting width of the structure. It is interpreted here that the structure ends just before the uplift at the trailing edge, which fixes these parameters. The inferred fault displacement is larger than the offset of marker 3 at the fault tip, indicating that the fault had a normal separation prior to shortening. Thus the rotated block is an inversion structure. The only other inverted faults are at the trailing edge of the rotated block, in the location where shortening might be expected due to the predicted excess area (Eq. 11.47). The measured excess area (3.01 km^2) is in reasonable agreement with that predicted from the fault geometry and amount of rotation (3.23 km^2).

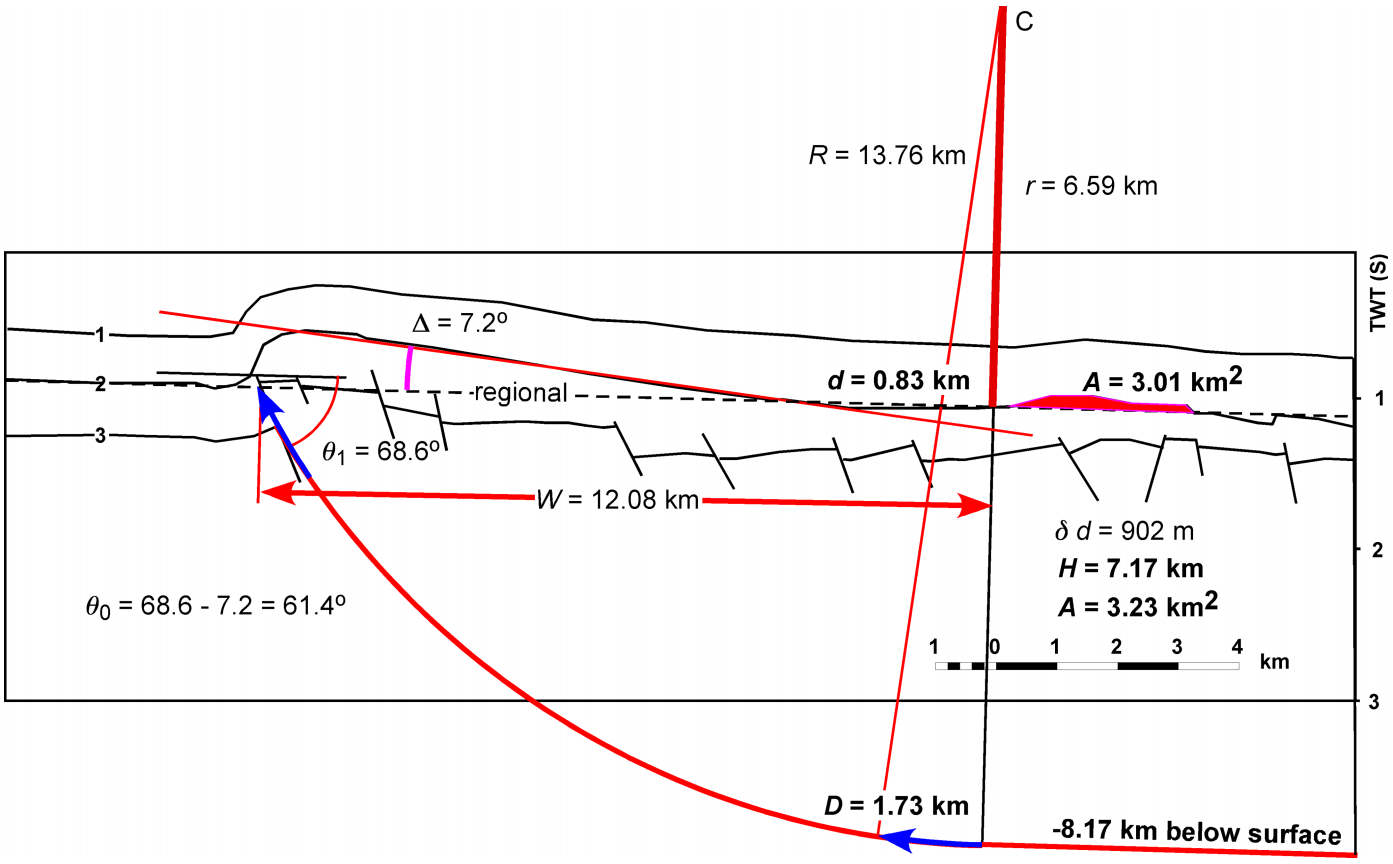

Fig. 11.73A. Rigid-block interpretation of South Hewett fault zone. Interpreted geometry in *red*, interpreted displacement on fault in *blue*

The simple shear method is an appropriate restoration technique for a half graben. The cross section in Fig. 11.74 restores well with vertical simple shear, validating the cross section.

The hangingwall of the Schell Creek fault (Fig. 11.75) is an internally deformed half graben in which the deformation mechanism is brittle extension by conjugate normal faults and domino-block rotation. Oblique simple shear is an appropriate technique for predicting the depth to detachment. The original reference line that is assumed to have been horizontal prior to formation of the half graben is the NSRD, the northern Snake Range detachment. The strain (17.8%) in the part of the rollover with the most detailed interpretation (Fig. 11.75Aa) is assumed to be representative of the entire rollover. The shear angle computed from Eq. 11.48 is 66°. The rollover shape is found with the oblique simple shear construction (Fig. 11.75Ab,c). The shape of the rollover adjacent to the master fault is independent of the choice of the original regional, but the depth to detachment strongly depends on the choice. If the regional is at the current position of the NSRD, the lower detachment is at –4 km below sea level (Fig. 11.75Ab), the location inferred by Gans et al. (1985). If the regional was higher than the present-day elevation, the master fault continues to slope downward across the entire cross section as inferred from a deep seismic profile by Hauser et al. (1987).

Fig. 11.75A.
Schell Creek fault (modified from Groshong 1989). **a** Data. **b** Interpretation if regional is at present-day location of NSRD (northern Snake Range detachment). **c** Interpretation if regional is above the present-day elevation